

Research Paper

Multicolor Upconversion Nanoparticles for Protein Conjugation

Stefan Wilhelm¹, Thomas Hirsch¹, Wendy M. Patterson¹, Elisabeth Scheucher², Torsten Mayr², Otto S. Wolfbeis¹,

1. University of Regensburg, Institute of Analytical Chemistry, Chemo- and Biosensors, 93040 Regensburg, Germany.

2. Graz University of Technology, Institute of Analytical Chemistry and Food Chemistry, 8010 Graz, Austria.

 Corresponding author: otto.wolfbeis@ur.de; www.wolfbeis.de.© Ivyspring International Publisher. This is an open-access article distributed under the terms of the Creative Commons License (<http://creativecommons.org/licenses/by-nc-nd/3.0/>). Reproduction is permitted for personal, noncommercial use, provided that the article is in whole, unmodified, and properly cited.

Received: 2012.08.27; Accepted: 2012.09.23; Published: 2013.03.13

Abstract

We describe the preparation of monodisperse, lanthanide-doped hexagonal-phase NaYF₄ up-converting luminescent nanoparticles for protein conjugation. Their core was coated with a silica shell which then was modified with a poly(ethylene glycol) spacer and N-hydroxysuccinimide ester groups. The nanoparticles were characterized by transmission electron microscopy, Raman spectroscopy, X-ray diffraction, and dynamic light scattering. The N-hydroxysuccinimide ester functionalization renders them highly reactive towards amine nucleophiles (e.g., proteins). We show that such particles can be conjugated to proteins. The protein-reactive UCLNPs and their conjugates to streptavidin and bovine serum albumin display multicolor emissions upon 980-nm continuous wave laser excitation. Surface plasmon resonance studies were carried out to prove bioconjugation and to compare the affinity of the particles for proteins immobilized on a thin gold film.

Key words: Upconversion luminescence, nanoparticle, silica coating, Raman spectroscopy, bio-sensing, magnetic separation, surface plasmon resonance.

Introduction

The implementation of nanotechnology to healthcare holds great promise in areas such as imaging [1,2,3,4,5], faster diagnosis [6], targeting [7], drug delivery [8], and tissue regeneration [9], as well as the development of medical products [10,11,12]. The chemical synthesis of NPs has been studied in detail during the last decade [13,14,15,16]. Substantial efforts have been made to control the dimensions, shape, composition, particle size distribution, etc., of NPs, thereby creating new materials with size dependent electrical, optical, magnetic, catalytic, and chemical properties, which cannot be achieved by their bulk counterparts. Important classes of NPs are a) magnetic NPs, b) gold NPs, c) quantum dots, d) silica NPs, etc. [17,18,19,20,21,22,23]. In recent years,

upconverting luminescent nanoparticles (UCLNPs) joined this classification. Photon upconversion has been researched ever since the 1960s. It is a process where two or more photons are sequentially absorbed, resulting in the emission of light at a shorter wavelength than the excitation light. For instance, infrared or near-infrared (NIR) light can be converted to shorter-wavelength radiation, usually in the visible range of the electromagnetic spectrum (anti-Stokes type emission) [24].

The mechanisms behind photon upconversion were first investigated in lanthanide-doped bulk materials by Auzel, Ovsyankin, and Feofilov [25]. In a sensitizer/activator system, the excitation energy is absorbed by a sensitizer ion (e.g., Yb³⁺) and trans-

ferred to an activator ion (e.g., Er^{3+} or Tm^{3+}) via a non-radiative, resonant energy transfer process. Metastable, long-lived energy states are required, in which case energy transfer upconversion (ETU) is possible, where the combined energies of pump photons are stored, which can lead to the emission of a higher energy photon [26].

Anti-Stokes emissions from UCLNPs offer several advantages over conventional Stokes-shifted emissions from a) semiconductor quantum dots, b) organic- and protein-based fluorophores, and c) the multiphoton process employing fluorescent dyes. UCLNPs are very attractive phosphors in terms of bioimaging due to their nonblinking emission and remarkable photostability [27,28,29]. In biological samples or tissue, there is minimal excitation of autofluorophores, since UCLNPs are usually excited by NIR (980 nm) continuous wave (cw) laser light. This scheme enables luminescence to be imaged with a high signal to noise ratio, minimizes possible photo-damage in biological systems, and allows deeper tissue penetration [30,31]. Upconversion microparticles have been used before in immunoassays [32] and enzyme activity assays [33], but their size (1 – 10 μm) and large size distribution makes their use less attrac-

tive. With respect to the relative size of a protein and upconversion *microparticles*, one may not speak of a label in its classical sense.

High-quality UCLNPs (with respect to crystal phase, monodispersity, geometry, etc.) are usually synthesized in high-boiling organic solvents (e.g., 1-octadecene) using ligand molecules with long alkyl chains (e.g., oleic acid), which renders them inherently functionalized with hydrophobic alkyl groups and only dispersible in non-polar organic solvents such as toluene, hexane, and the like [34,35]. In order to make them amenable to bioanalytical applications, surface modification is required, to make the UCLNPs water dispersible, offering a platform for further conjugation of functional chemical groups and/or (bio)-molecules. Silica is known for its biocompatibility [36], and silica coating of UCLNPs therefore offers an attractive way of functionalization [37,38]. This has already been applied to a multitude of nanoparticle systems, including gold and silver NPs [39], magnetic NPs [40], and quantum dots [41]. In addition, silica coating is a flexible coating technique that is applicable to both hydrophilic and hydrophobic NPs [42,43,44]. The coating process of hydrophilic NPs relies on the Stöber method, while a reverse-microemulsion method is typically used for coating hydrophobic NPs [45].

We describe the synthesis of protein-reactive, multicolor UCLNPs. First, monodisperse, lanthanide-doped hexagonal-phase NaYF_4 nanoparticles were prepared, which were coated with oleic acid, as can be seen in Scheme 1.

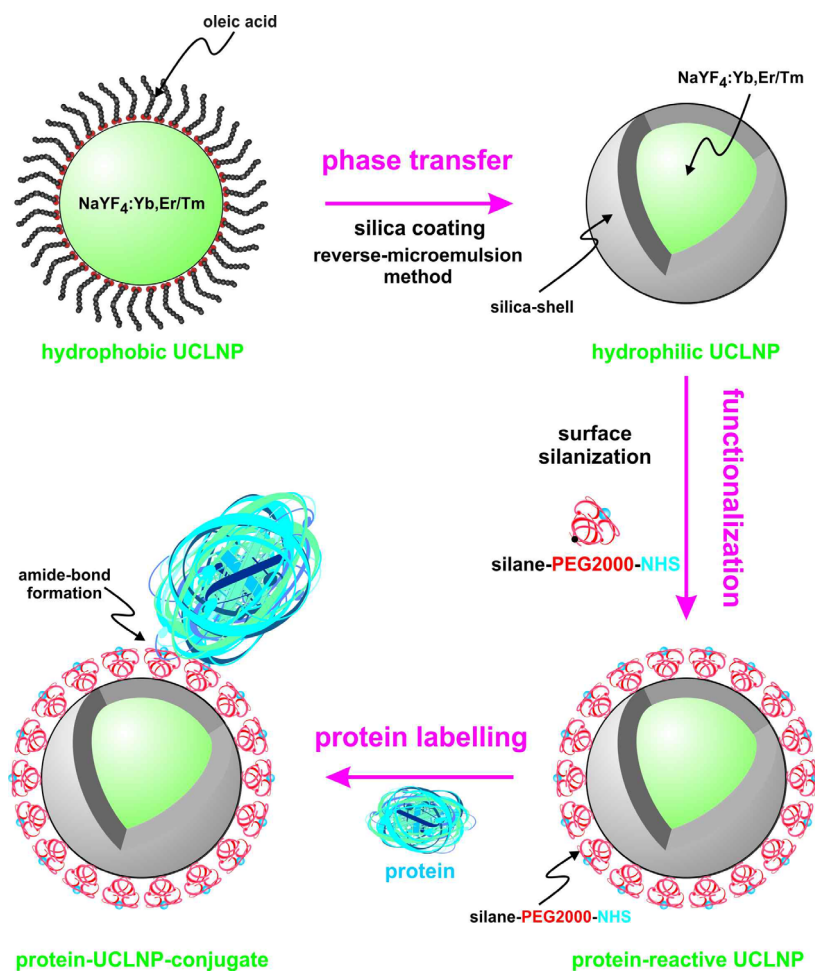


Figure S1. (Scheme 1). Surface engineering of UCLNPs towards protein-reactive, multicolor upconverting labels.

In the second step, the particles were silica coated using a reverse-microemulsion method, and subsequently functionalized with an amino-reactive silanization reagent. This reagent consists of a triethoxysilane conjugated to a poly(ethylene glycol) spacer (PEG) and a carboxyl group activated with an N-hydroxysuccinimide (NHS) ester. The NHS ester of the silica-coated UCLNPs renders them highly reactive towards proteins. The protein-reactive UCLNPs exhibit multicolor

luminescence emission after 980-nm laser excitation. Finally, surface plasmon resonance (SPR) studies were carried out to study the binding affinity of NHS-activated nanoparticles to proteins that previously were immobilized on a gold film.

Materials and Methods

Chemicals

Yttrium(III) chloride hexahydrate (99.99%), ytterbium(III) chloride hexahydrate (99.9%), erbium(III) chloride hexahydrate (99.9%), thulium(III) chloride hexahydrate (99.99%), ammonium fluoride (ACS reagent $\geq 98.0\%$), sodium hydroxide (reagent grade $\geq 98.0\%$), Igepal® CO-520, tetraethyl orthosilicate (TEOS), bovine serum albumin (BSA) fraction V (purity $>96\%$), 16-mercapto-hexadecanoic acid (95%), N-(3-dimethylaminopropyl)-N'-ethylcarbodiimide hydrochloride (EDC) commercial grade, and sodium chloride (p.A.) were purchased from Sigma-Aldrich (www.sigmaaldrich.com), oleic acid (technical grade 90%) and 1-octadecene (technical grade 90%) from Alfa Aesar (www.alfa.com), triethoxysilane poly(ethylene glycol) 2000 succinimidyl ester from Nanocs (www.nanocs.com), ammonia solution (32%), 2-propanol (p.A.), 2-amino-2-hydroxymethylpropane-1,3-diol (TRIS, molecular biology grade), from Merck (www.merckgroup.com), sodium hydrogen carbonate (p.A.) from Ferak (www.ferak.de), ethanol (p.A.) from Roth (www.carloth.de), and streptavidin-modified magnetic beads (PureProteome™) from Millipore (www.millipore.com). All other reagents and organic solvents were of the highest grade available.

Instrumentation

Transmission electron microscopy (TEM) was performed using a 120 kV Philips CM12 (www.fei.com) microscope. Upconversion luminescence spectra were recorded with a luminescence spectrometer (LS 50 B) from Perkin Elmer (www.perkinelmer.com), modified with a 980-nm cw laser (120 mW) from Roithner (www.roithner-laser.com) for upconversion photo-excitation. All centrifugation steps were carried out in a Hettich Universal 320 centrifuge (www.hettichlab.com). Raman spectroscopy was performed using a DXR Raman microscope from Thermo Scientific (www.thermoscientific.com) with 532-nm cw laser excitation (8 mW). The Zetasizer Nano ZS from Malvern (www.malvern.com) was used for dynamic light scattering (DLS) experiments. X-ray powder diffraction (XRD) patterns with a resolution of 0.02° (2θ) were collected using a Stoe Stadi P

diffractometer (www.stoe.com) with a Cu source (K α radiation, $\lambda=1.54060 \text{ \AA}$) operating at 40 kV and 42 mA. All SPR experiments were performed with a Biosuplar 6 instrument from Mivitec GmbH, (www.biosuplar.com). Typically, glass slides with a 50 nm thick gold film were used, and intensity measurements were performed at constant angle. The signal intensity was calibrated in refractive index units (RIU) with solutions of sodium chloride of different concentrations and known refractive index.

Synthesis of hydrophobic NaYF₄ nanoparticles doped with Yb/Er or Yb/Tm

Two systems of hydrophobic, lanthanide-doped NaYF₄ nanocrystals were prepared via a modified procedure as reported by Zhang et al. [46]. For the first system YCl₃·6H₂O (0.747 mmol), YbCl₃·6H₂O (0.25 mmol), TmCl₃·6H₂O (0.003 mmol) were employed. In the second system YCl₃·6H₂O (0.78 mmol), YbCl₃·6H₂O (0.20 mmol), ErCl₃·6H₂O (0.02 mmol) were used. The salts were dissolved in approximately 5 mL of methanol by sonication. The respective clear and optically transparent solution of rare earth chlorides in methanol was transferred into a 50 mL flask, mixed with 8 mL of oleic acid and 15 mL of 1-octadecene under an atmosphere of nitrogen and heated to 160 °C. A homogeneous, clear solution was formed after 30 minutes at 160 °C under vacuum. The reaction mixture was then cooled to room temperature and 10 mL of methanol containing NaOH (0.25 M) and NH₄F (0.4 M) were added at once. The colloidal dispersion was heated to 120 °C and stirred for 30 minutes. The resulting colloid was refluxed at approximately 325 °C for 15 minutes. After cooling to room temperature, the UCLNPs were precipitated by addition of approximately 20 mL of ethanol and isolated via centrifugation at a relative centrifugal force (RCF) of 1000 g for 5 minutes. The pellet was washed several times by dispersing it in small amounts (approximately 0.5 mL) of chloroform and cyclohexane, then precipitating them by the addition of a large excess (approximately 15 mL) of ethanol and acetone. A white solid was obtained, which can be easily re-dispersed in cyclohexane to form a clear dispersion. This was used for further silica coating.

Silica coating of hydrophobic nanoparticles

The surface of the hydrophobic UCLNPs was coated with silica using a modified reverse-microemulsion technique [36]. 10 mg of the UCLNPs were dispersed in 10 mL of cyclohexane in a 25 mL round bottom flask. Then, 500 μ L of Igepal® CO-520 and 80 μ L of an aqueous ammonia solution (32%) were added. This yielded a clear and stable

emulsion after 30 minutes of sonication, which was supplemented with 60 μL (0.27 mmol) of TEOS and kept for 24 hours at room temperature under magnetic stirring (600 rpm). The silica-coated UCLNPs were collected via centrifugation (RCF 3000 g for 5 minutes). Three cycles of re-dispersion and centrifugation were performed to wash the pellet with an ethanol/water mixture (1:1 v/v). The nanoparticles were filtered through a syringe filter with a pore size of 200 nm and stored in ethanol.

Functionalization of silica-coated nanoparticles

A fresh solution of 10 mg of triethoxysilane poly(ethylene glycol) 2000 succinimidyl ester in 500 μL of ethanol was added to a dispersion of 3 mg of silica-coated UCLNPs in 200 μL ethanol. The mixture was magnetically stirred for 2 hours at room temperature. The succinimidyl-functionalized UCLNPs were collected via centrifugation (RCF 17000 g for 10 minutes), and the unreacted materials were washed away with cold distilled water. Thereafter, the succinimidyl-functionalized UCLNPs were stored in 2-propanol at 4 $^{\circ}\text{C}$.

Conjugation of succinimidyl-functionalized nanoparticles to streptavidin-modified magnetic beads

An aliquot (100 μL) of a dispersion of the magnetic beads was placed in a microcentrifuge tube. The magnetic beads were collected with a permanent magnet and washed two times with a hydrogen carbonate buffer (HCB) solution (0.1 M) adjusted to pH 9 with 1 M NaOH. After washing, the magnetic beads were dispersed in 500 μL of HCB. In parallel, 1 mg of succinimidyl-functionalized UCLNPs in 500 μL of 2-propanol was collected via centrifugation (RCF 17000 g for 10 minutes). The supernatant was discarded and 500 μL of HCB were added to the pellet. An optically transparent dispersion was obtained after sonication. The dispersions of streptavidinylated magnetic beads and protein-reactive UCLNPs were combined and magnetically stirred at room temperature for 2 hours. The streptavidin-modified magnetic bead UCLNPs conjugate was collected with a permanent magnet and washed two times with HCB.

Conjugation of succinimidyl-functionalized nanoparticles to bovine serum albumin

A self-assembled monolayer of a carboxy-terminated alkane thiol was prepared by immersing a gold glass slide overnight in a solution of 16-mercapto-hexadecanoic acid (400 μM) in ethanol. The protein (BSA) was bound to this surface via EDC

coupling [47]. First, 20 mg of BSA were dissolved in 10 mL aqueous NaCl solution (140 mM). Second, 480 mg of EDC were added and mixed by vortexing. This solution was applied to the SPR chip. The binding of BSA to the activated carboxy groups was monitored in real time by SPR. Changes in the intensity of the reflected light were recorded at constant angle. An increase in the intensity of the SPR signal over time indicated binding of BSA. Saturation had occurred after approximately 30 minutes. The chip was washed with a solution of sodium chloride (140 mM). Again, BSA together with EDC was loaded onto the chip. Only a slight increase in the signal could be observed. After washing, the signal returned to the starting values (prior to the second immobilization). This indicates that surface modification with BSA was successful. Next, the solution in the SPR cell was changed to HCB. When the signal reached a constant value, protein-reactive UCLNPs (1 mg/mL) in HCB were added. After 80 minutes, no significant increase in the SPR signal was observed. Washing steps with hydrochloric acid (0.1 M) for 10 minutes and with HCB for 10 minutes led to a decrease in the signal by approximately 20%.

Results and Discussion

The hydrophobic NaYF_4 nanoparticles doped with Yb/Er and Yb/Tm possess good monodispersity and hexagonal crystal phase. They were prepared via a modification of a known method [46]. The doping concentrations of lanthanide ions are 20/2 mol% for doping with Yb/Er, and 25/0.3 mol% for doping with Yb/Tm. Lanthanide-doped β -phase NaYF_4 displays superior brightness compared to other host materials [48], which is about one order of magnitude better than comparable cubic α -phase NaYF_4 UCLNPs [46,49]. The upconversion luminescence spectra of the corresponding Yb/Er and Yb/Tm-doped samples acquired from dispersions in cyclohexane are displayed in Figure 1A. Under 980-nm cw laser excitation, the $\text{NaYF}_4(20\%\text{Yb}/2\%\text{Er})$ nanocrystals yield three distinct emission peaks at 522, 541, and 655 nm. These are assigned to the $^4\text{H}_{11/2} - ^4\text{I}_{15/2}$, $^4\text{S}_{3/2} - ^4\text{I}_{15/2}$, and $^4\text{F}_{9/2} - ^4\text{I}_{15/2}$ transitions of Er^{3+} ions, respectively [45].

The spectrum of $\text{NaYF}_4(25\%\text{Yb}/0.3\%\text{Tm})$ displays two blue emission peaks (450 and 475 nm), which correspond to the $^1\text{D}_2 - ^3\text{F}_4$ and $^1\text{G}_4 - ^3\text{H}_6$ transitions of the Tm^{3+} ions, respectively. Additionally, there are two weaker peaks at 646 nm ($^3\text{F}_2 - ^3\text{F}_3$) and 696 nm ($^3\text{H}_6 - ^1\text{G}_4$) [45]. The predominantly blue and green emissions of optically transparent colloidal dispersions of the corresponding multicolor nanoparticles in cyclohexane upon 980-nm cw laser excitation

can be seen in Figure 1B. It shall be mentioned here that the luminescence of UCLNPs strongly depends on temperature and, in fact, has been used to sense it on a nanoscale [50].

Dispersions of the UCLNPs in cyclohexane exhibit very good colloidal stability. No sedimentation or agglomeration was found even after several weeks. Dynamic light scattering (DLS) experiments performed at 25 °C with a 632.6-nm laser and a non-invasive backscatter technique confirmed this observation. The average hydrodynamic diameter of the Yb/Er-doped nanoparticles is 34.4 nm, with a full-width at half maximum (FWHM) of 5 nm, this yielding a polydispersity index (PI) of 0.072. The respective values for the Yb/Tm-doped UCLNPs are 31.8 nm for the diameter, 5.3 nm FWHM, and a PI of 0.048. Excellent correlation statistics and fits (data not shown) were obtained using a non-negative least squares analysis algorithm.

The TEM images of the corresponding nanocrystals are shown in Figure 2. A dispersion of UCLNPs in cyclohexane was dried on a carbon-coated copper grid. The roughly spherical nanoparticles form a 2D hexagonal closed packing, as can be seen from the TEM images. This behavior may be due to van-der-Waals interaction of oleic acid (OA) molecules on the particles' surface and the solid carbon support of TEM grids. The average particle diameters as determined via TEM are 27 nm for the Yb/Er-doped sample and 25 nm for the Yb/Tm-doped sample. These results are in good

agreement with the DLS data, since DLS experiments take account of the hydrodynamic diameter of the particles rather than their sheer particle size.

The results of XRD crystal phase analyses are shown in Figure 2C, and demonstrate the high crystallinity of the UCLNPs. The XRD patterns of the two samples of nanocrystals are in good agreement with the standard pattern of β -NaYF₄ (ICDD PDF 16-334). Raman spectroscopy was used to characterize the phonon bands of the NaYF₄ nanocrystals (Figure 3A). They are clearly visible and distinct between 225 - 450 cm⁻¹. The weighed average of the phonon modes is 304 cm⁻¹ for the Yb/Er-doped sample, and 320 cm⁻¹ for the Yb/Tm-doped sample. This phonon energy is considerably lower than that of comparable fluoride host lattices such as LiYF₄ (570 cm⁻¹) [51,52]. Additionally, it is predictably lower than that of bulk, un-doped NaYF₄ (360 cm⁻¹) [53] due to the modified phonon density of states [54]. Oleic acid has a distinct Raman spectrum in the 2830 - 2960 cm⁻¹ region where CH₂ stretching modes are observed. These are particularly susceptible to thermal changes, and slight spectral variations are expected from sample to sample for this reason [55]. The Raman spectra for this spectral region are shown in Figure 3B. Additional evidence of the presence of OA is exhibited by the strong CH₂ scissoring modes in the 1438 - 1456 cm⁻¹ region (not shown here). Other (but much weaker) Raman peaks for oleic acid can be observed in the 600 - 1800 cm⁻¹ region.

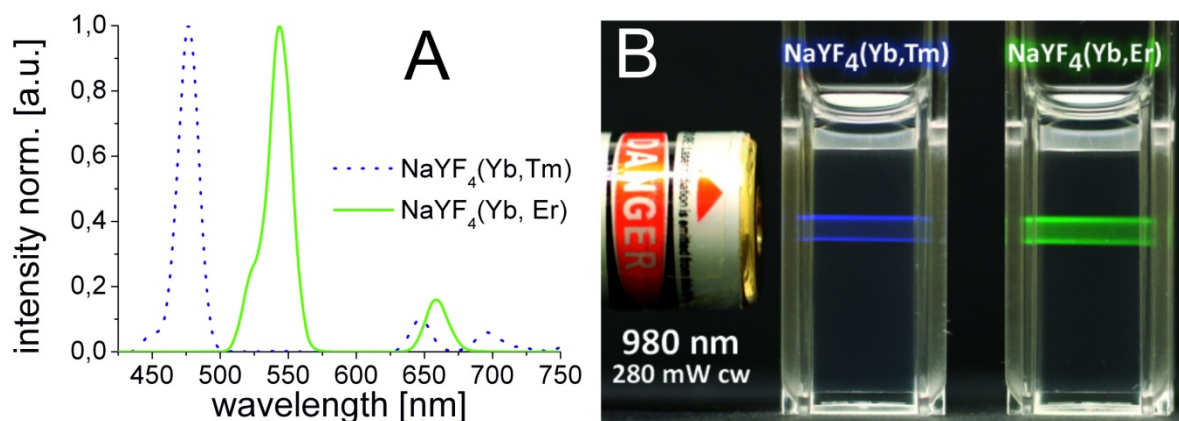


Figure 1. (A) Normalized upconversion luminescence spectra of Yb/Tm (dotted blue line) and Yb/Er-doped (solid green line) multicolor β -NaYF₄ nanocrystals. The UCLNPs were dispersed in cyclohexane (1 mg/mL). (B) Digital photograph of optically transparent colloidal dispersions of corresponding UCLNPs (1 mg/mL) in cyclohexane. The predominantly blue and green emissions of Yb/Tm and Yb/Er-doped UCLNPs upon 980-nm cw laser excitation can easily be seen by the bare eye.

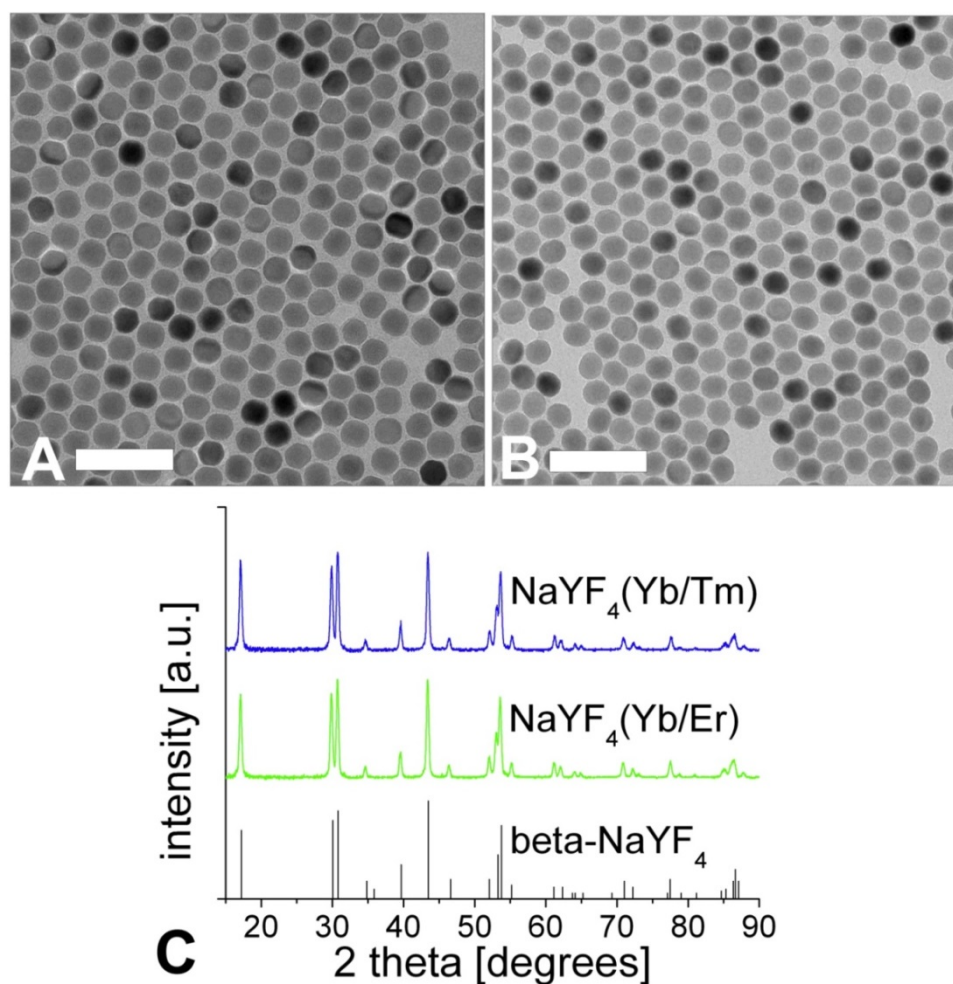


Figure 2. TEM images of $\text{NaYF}_4(20\%\text{Yb}/2\%\text{Er})$ (A) and $\text{NaYF}_4(25\%\text{Yb}/0.3\%\text{Tm})$ (B) upconversion luminescent nanoparticles, respectively. Scale bar: 100 nm. Graph (C) shows the corresponding XRD patterns and the standard XRD pattern of $\beta\text{-NaYF}_4$ (ICDD PDF 16-334).

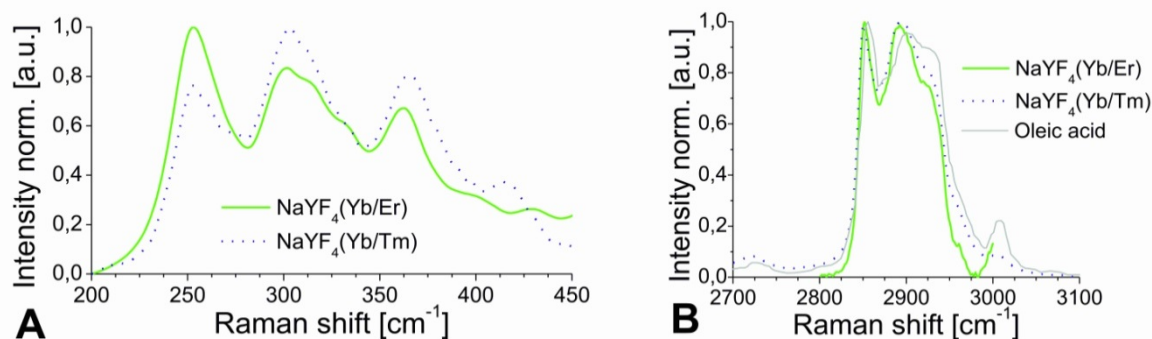


Figure 3. Raman spectra of UCLNPs focusing on the NaYF_4 phonon region (A), and the CH_2 stretching corresponding to the functionalized OA (B). The dotted blue line corresponds to the Yb/Tm-doped sample and the solid green line to the Yb/Er-doped UCLNPs. The Raman spectrum of pure, non-functionalized OA (solid grey line) is shown in (B) for comparison. The slight peak shifts and difference in peak widths between the non-functionalized OA and the OA-functionalized UCLNPs indicate that OA is likely to be bound to the surface of UCLNPs.

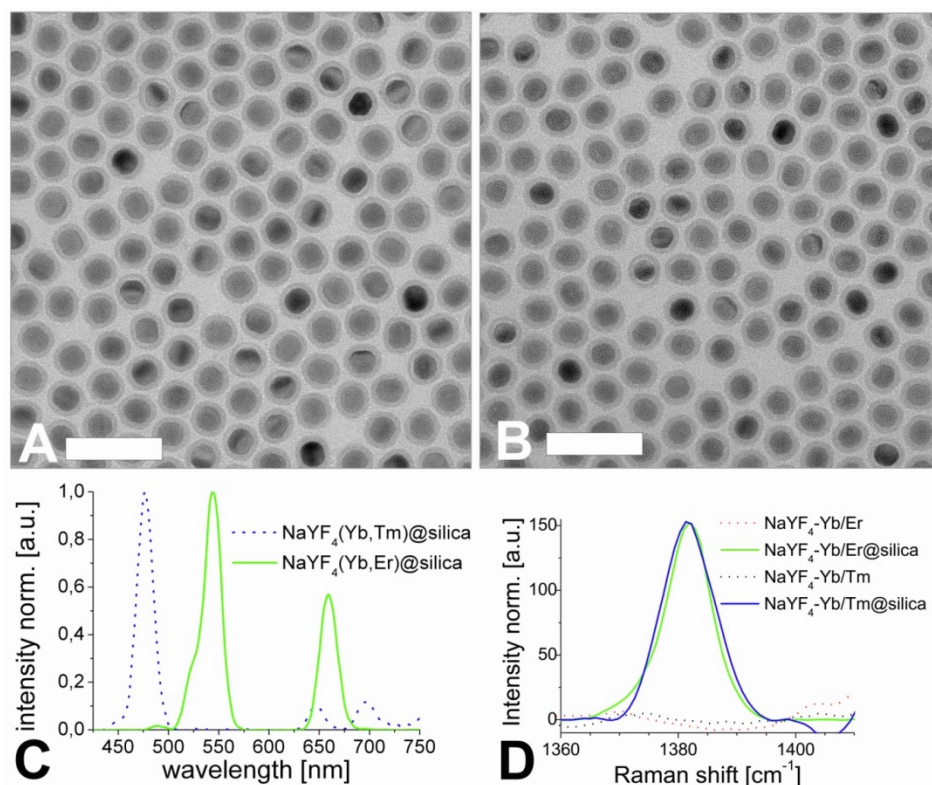


Figure 4. TEM images of silica-coated upconversion luminescent nanoparticles (UCLNPs) of the type $\text{NaYF}_4(20\% \text{Yb}/2\% \text{Er})@ \text{silica}$ (**A**) and of the type $\text{NaYF}_4(25\% \text{Yb}/0.3\% \text{Tm})@ \text{silica}$ (**B**) in water (1 mg/mL) before functionalization with PEG2000-NHS. The sample was prepared by dropping an aliquot of approximately 2 μL of silica-coated UCLNPs dispersion onto the surface of a carbon-coated copper grid. Scale bar: 100 nm. The normalized upconversion luminescence spectra of silica-coated Yb/Tm (dotted blue line) and Yb/Er-doped, $\beta\text{-NaYF}_4$ nanocrystals (solid green line) are shown in (**C**). The Raman spectra of UCLNPs with silica (solid lines) and without silica (dotted lines) are shown in (**D**). The same conditions were maintained in all experiments.

The hydrophobic, oleic acid-coated UCLNPs were then silica coated via a reverse-microemulsion technique according to a modified literature method [36]. This makes them water dispersible and biocompatible, which is a prerequisite for almost any bioapplications. The TEM images in Figure 4 demonstrate that this technique yields a thin and uniform silica coating on the hydrophobic nanoparticles. The formation of a silica shell can be clearly deduced from the TEM images, because silica exhibits an electron optical contrast which is quite different from that of rare earth-doped nanocrystals. The size of the Yb/Er-doped nanoparticles increased from 27 to 38 nm after silica coating, implying a shell thickness of approximately 5 nm. The diameter of the respective Yb/Tm-doped particles increased from 25 to 38 nm, and this corresponds to a shell thickness of about 6 nm.

The normalized upconversion luminescence spectra of Yb/Er and Yb/Tm-doped, silica coated, multicolor particles dispersed in deionized water solution are shown in Figure 4C. The silica-coated

nanocrystals also exhibit a Raman peak at 1381 cm^{-1} as shown in Figure 4D. This band is not present for the uncoated nanoparticles, and is likely to be due to the Si-CH₂ scissoring mode [56].

In the next step, a silane reagent with a PEG2000 spacer and activated as an N-hydroxysuccinimide (NHS) ester was covalently bound to the surface via a silanization technique [57]. The PEG spacer is beneficial in that it can prevent agglomeration, reduce un-specific binding, and improve solubility in water. The NHS ester groups render the silica-coated UCLNPs highly reactive towards proteins, as shown by labeling of streptavidin-modified magnetic beads.

We have attempted to calculate the number of NHS groups on a nanocrystal. In order to do so, the following assumptions have been made: (a) The average radius of the nanocrystals is 19 nm.

(b) The average radius of a (spherical) PEG 2000 molecule is approximately 1.5 nm [58]. The volume of a spherical nanocrystal with a radius of 19 nm can be calculated to be $29 \mu\text{m}^3$, and the volume of a spherical PEG 2000 molecule with a radius of 1.5 nm to be 14

nm³. The total volume of a spherical nanocrystal loaded with PEG 2000 is 45 μm³. The number of PEG 2000 molecules can be calculated if the difference (45 μm³ - 29 μm³) is divided by 14 nm³ and yields about 1100 NHS groups per (spherical) silica coated nanocrystal. We have to stress here that this is a rough number only and also presume that the number of NHS groups per nanocrystal can be governed (reduced) by using mixtures of PEG2000-NHS reagent and PEG2000-modified silyl reagent (without NHS groups), but this has not been verified experimentally.

Two sets of experiments were carried out. In a first (positive control) experiment, the streptavidinylated magnetic beads were mixed with UCLNP NHS esters in a conjugation buffer (HCB) of pH 9. After 2 hours at room temperature, the magnetic beads were collected with a permanent magnet and washed with HCB. The collected spot of streptavidin-modified

magnetic beads was identified by its upconversion luminescence upon 980-nm cw laser excitation (Figure 5A). This proves that the protein-reactive multicolor UCLNPs bind to streptavidin. In a second (negative control) experiment, the UCLNP NHS esters were previously deactivated by reacting them with the amino groups of TRIS buffer solution (2 mM, pH 8.5) overnight at room temperature. The first experiment was then repeated with the deactivated nanoparticles. Indeed, the upconversion luminescence of the collected cluster of streptavidin-modified magnetic beads was not observed. This fact proves that the deactivated particles are not bound to the streptavidinylated magnetic beads. On the other hand, a dispersion of the unreactive particles also display upconversion emission upon 980-nm cw laser excitation (Figure 5B).

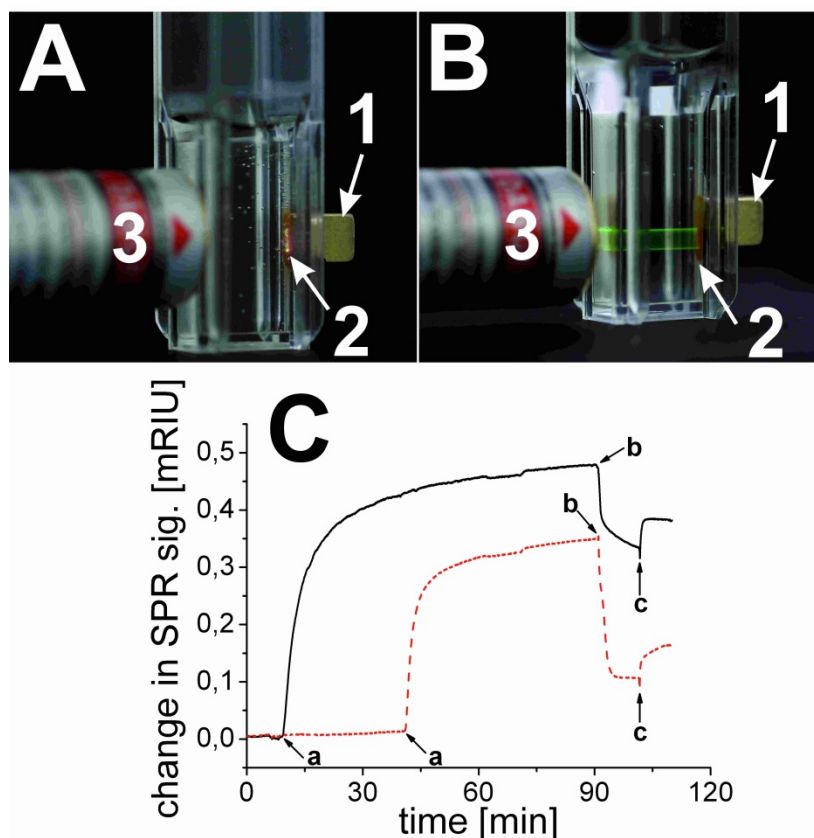


Figure 5. (A; top) Digital photograph of the protein-reactive upconversion luminescent nanoparticles (UCLNPs) bound to streptavidin-modified magnetic beads (2), collected with a permanent magnet (1) upon 980-nm cw laser (3) excitation (280 mW) in a hydrogen carbonate buffer. (B; top) Photograph illustrating that UCLNP NHS esters that were deactivated by reaction with Tris buffer and dispersed in a hydrogen carbonate buffer do not bind to streptavidinylated magnetic beads (2). (C; bottom) SPR results showing the unspecific binding of deactivated UCLNPs (dotted red line) and specific binding of protein-reactive UCLNPs (solid black line) to BSA immobilized on a gold substrate. The curves show the addition of the respective UCLNPs in a hydrogen carbonate buffer (a), and the washing steps with hydrochloric acid (0.1 M, b), and hydrogen carbonate buffer solution (c).

In order to quantitatively verify the functionality of protein-reactive nanoparticles, their binding to surface-immobilized BSA was monitored by SPR measurements in real time. SPR provides a well-known label free method to study interaction of biomolecules on thin gold films [59]. We coated the thin gold surface with a monolayer of a carboxy-terminated alkanethiol. The protein was immobilized via EDC coupling onto this surface. The binding of protein-reactive NPs to BSA was studied by measuring the shift in the surface plasmon resonance. Therefore, one can either measure the angle of minimum reflection of the light as a function of time, or monitor the time-dependent change in the intensity of the reflected light at a constant angle of incidence. The kinetics for binding of the nanoparticles to the protein layer can be seen in Figure 5C. Both the protein-reactive and the deactivated UCLNPs bind to BSA. After washing with 0.1 mM hydrochloric acid for 10 minutes and then with hydrogen carbonate buffer for another 10 minutes, it can be clearly seen that the protein-reactive particles still bind quite strongly. Some deactivated particles also bind due to non-specific binding. On the other hand, when using nanoparticles with a silica shell without NHS groups, we also see unspecific binding, but the particles can be simply washed off with buffer.

Conclusion

We report here on the preparation of monodisperse, multicolor UCLNPs with controlled diameters of ~26 nm using a modified solvothermal method. In order to make them amenable to bioanalytical applications, surface modification was performed by first depositing a thin silica shell (~5 nm thick) on the hydrophobic nanoparticles, this followed by coating it with a poly(ethylene glycol) spacer carrying N-hydroxysuccinimide groups. The resulting particles form stable dispersions in aqueous solution and are highly reactive towards proteins such as streptavidin and bovine serum albumin. Such amino-reactive labels form an attractive alternative to thiol-reactive UCLNPs [60]. Specifically, the reactive UCLNPs were conjugated to streptavidin-modified magnetic beads. The magnetic beads labeled with streptavidinylated UCLNPs were separated by magnetic force and displayed upconversion luminescence upon 980-nm laser excitation. We believe that such amino-reactive multicolor nanoparticles can be employed as luminescent labels for various kinds of (organic) amines, biogenic amines, proteins, or amino-modified oligomers. Labeled proteins have numerous applications such as in immunoassays, enzymatic assays, and in imaging. All these will strongly

benefit from the use of labels with photon upconversion capability.

Acknowledgements

This work was part of a project of the German Research Foundation (DFG) and supported within the DFG funding program *Open Access Publishing*. Furthermore, the authors thank Dr. Martina Andratschke for performing the XRD measurements and Sandy F. Himmelstoss for SPR measurements.

Competing Interests

The authors have declared that no competing interests do exist.

References

- 1 Lee J-H, Huh Y-M, Jun Y, Seo J, Jang J, Song H-T, et al. Artificially engineered magnetic nanoparticles for ultra-sensitive molecular imaging. *Nature Medicine*. 2007; 13 (1): 95-9.
- 2 Medintz IL, Uyeda HT, Goldman ER, Mattoussi H. Quantum dot bioconjugates for imaging, labelling and sensing. *Nature Materials*. 2005; 4 (6): 435-46.
- 3 Michalet X, Pinaud FF, Bentolila LA, Tsay JM, Doose S, Li JJ, et al. Quantum dots for live cells, in vivo imaging, and diagnostics. *Science*. 2005; 307 (5709): 538-544.
- 4 Hilderbrand SA, Shao F, Salthouse C, Mahmood U, Weissleder R. Up-converting luminescent nanomaterials: application to in vivo bioimaging. *Chemical Communications*. 2009; (28): 4188-90.
- 5 Mader HS, Kele P, Saleh SM, Wolfbeis OS. Upconverting luminescent nanoparticles for use in bioconjugation and bioimaging. *Current Opinion in Chemical Biology*. 2010; 14 (5): 582-96.
- 6 Agasti SS, Rana S, Park M-H, Kim CK, You C-C, Rotello VM. Nanoparticles for detection and diagnosis. *Advanced Drug Delivery Reviews*. 2010; 62 (3): 316-28.
- 7 von Maltzahn G, Park J-H, Lin KY, Singh N, Schwöppe C, Mesters R, et al. Nanoparticles that communicate in vivo to amplify tumour targeting. *Nature Materials*. 2011; 10 (7): 545-52.
- 8 Zrazhevskiy P, Sena M, Gao X. Designing multifunctional quantum dots for bioimaging, detection, and drug delivery. *Chemical Society Reviews*. 2010; 39 (11): 4326-54.
- 9 Wang H, Leeuwenburgh SCG, Li Y, Jansen JA. The use of micro- and nanospheres as functional components for bone tissue regeneration. *Tissue Engineering Part B: Reviews*. 2012; 18 (1): 24-39.
- 10 Davis ME, Zuckerman JE, Choi CHJ, Seligson D, Tolcher A, Alabi CA, et al. Evidence of RNAi in humans from systemically administered siRNA via targeted nanoparticles. *Nature*. 2010; 464 (7291): 1067-70.
- 11 Ma X, Zhao Y, Liang X-J. Theranostic nanoparticles engineered for clinic and pharmaceuticals. *Accounts of Chemical Research*. 2011; 44 (10): 1114-22.
- 12 Yong KT, Wang Y, Roy I, Rui H, Swihart MT, Law WC, Kwak SK, Ye L, Liu J, Mahajan SD, Reynolds JL. Preparation of quantum dot/drug nanoparticle formulations for traceable targeted delivery and therapy. *Theranostics*. 2012; 2 (7): 681-94.
- 13 Park J, An K, Hwang Y, Park J-G, Noh H-J, Kim J-Y, et al. Ultra-large-scale syntheses of monodisperse nanocrystals. *Nature Materials*. 2004; 3 (12): 891-5.
- 14 Frey NA, Peng S, Cheng K, Sun S. Magnetic nanoparticles: synthesis, functionalization, and applications in bioimaging and magnetic energy storage. *Chemical Society Reviews*. 2009; 38 (9): 2532-42.
- 15 Ye X, Collins JE, Kang Y, Chen J, Chen DTN, Yodh AG, et al. Morphologically controlled synthesis of colloidal upconversion nanophosphors and their shape-directed self-assembly. *Proceedings of the National Academy of Sciences*. 2010; 107 (52): 22430-5.
- 16 Singamaneni S, Bliznyuk VN, Binek C, Tsymbal EY. Magnetic nanoparticles: recent advances in synthesis, self-assembly and applications. *Journal of Materials Chemistry*. 2011; 21 (42): 16819-45.

- 17 Shao H, Min C, Issadore D, Liong M, Yoon TJ, Weissleder R, Lee H. Magnetic nanoparticles and microNMR for diagnostic applications. *Theranostics*. 2012; 2 (1): 55-65.
- 18 Gao J, Gu H, Xu B. Multifunctional magnetic nanoparticles: design, synthesis, and biomedical applications. *Accounts of Chemical Research*. 2009; 42 (8): 1097-107.
- 19 Boisselier E, Astruc D. Gold nanoparticles in nanomedicine: preparations, imaging, diagnostics, therapies and toxicity. *Chemical Society Reviews*. 2009; 38 (6): 1759-82.
- 20 Alivisatos AP, Gu W, Larabell C. Quantum dots as cellular probes. *Annual Review of Biomedical Engineering*. 2005; 7 (1): 55-76.
- 21 Liu L, Yong KT, Roy I, Law WC, Ye L, Liu J, Liu J, Kumar R, Zhang X, Prasad PN. Bioconjugated pluronic triblock-copolymer micelle-encapsulated quantum dots for targeted imaging of cancer: in vitro and in vivo studies. *Theranostics*. 2012; 2 (7): 705-13.
- 22 Zhuang Z, Peng Q, Li Y. Controlled synthesis of semiconductor nanostructures in the liquid phase. *Chemical Society Reviews*. 2011; 40 (11): 5492-513.
- 23 Zou H, Wu S, Shen J. Polymer/silica nanocomposites: preparation, characterization, properties, and applications. *Chemical Reviews*. 2008; 108 (9): 3893-957.
- 24 Vennerberg D, Lin Z. Upconversion nanocrystals: synthesis, properties, assembly and applications. *Science of Advanced Materials*. 2011; 3 (1): 26-40.
- 25 Auzel F. Upconversion and anti-stokes processes with f and d ions in solids. *Chemical Reviews*. 2004; 104 (1): 139-74.
- 26 Menyuk N. NaYF₄: Yb,Er - an efficient upconversion phosphor. *Applied Physics Letters*. 1972; 21 (4): 159-61.
- 27 Wu S, Han G, Milliron DJ, Aloni S, Altoe V, Talapin DV, et al. Non-blinking and photostable upconverted luminescence from single lanthanide-doped nanocrystals. *Proceedings of the National Academy of Sciences*. 2009; 106 (27): 10917-10921.
- 28 Park YI, Kim JH, Lee KT, Jeon K, Na HB, Yu JH, et al. Nonblinking and nonbleaching upconverting nanoparticles as an optical imaging nanoprobe and T1 magnetic resonance imaging contrast agent. *Advanced Materials*. 2009; 21 (44): 4467-71.
- 29 Wang F, Han Y, Lim CS, Lu Y, Wang J, Xu J, et al. Simultaneous phase and size control of upconversion nanocrystals through lanthanide doping. *Nature*. 2010; 463 (7284): 1061-5.
- 30 Achatz DE, Ali R, Wolfbeis OS. Luminescent chemical sensing, biosensing, and screening using upconverting nanoparticles. *Topics in Current Chemistry*. 2011, 300: 29-50.
- 31 Chen G, Shen J, Ohulchanskyy TY, Patel NJ, Kutikov A, Li Z, et al. (α-NaYbF₄:Tm³⁺)/CaF₂ core/shell nanoparticles with efficient near-infrared to near-infrared upconversion for high-contrast deep tissue bioimaging. *ACS Nano*. 2012; DOI: 10.1021/nr302972r.
- 32 Kuningas K, Ukonaho T, Pääkkilä H, Rantanen T, Rosenberg J, Lövgren T, et al. Upconversion Fluorescence Resonance Energy Transfer in a Homogeneous Immunoassay for Estradiol. *Analytical Chemistry*. 2006; 78 (13): 4690-6.
- 33 Rantanen T, Järvenpää M-L, Vuojola J, Kuningas K, Soukka T. Fluorescence-Quenching-Based Enzyme-Activity Assay by Using Photon Upconversion. *Angewandte Chemie*. 2008; 120 (20): 3871-3.
- 34 Abel KA, Boyer J-C, Veggel FCJM van. Hard proof of the NaYF₄/NaGdF₄ nanocrystal core/shell structure. *Journal of the American Chemical Society*. 2009; 131 (41): 14644-5.
- 35 Chen G, Ohulchanskyy TY, Kumar R, Ågren H, Prasad PN. Ultrasmall monodisperse NaYF₄:Yb³⁺/Tm³⁺ nanocrystals with enhanced near-infrared to near-infrared upconversion photoluminescence. *ACS Nano*. 2010; 4 (6): 3163-8.
- 36 Abdul Jalil R, Zhang Y. Biocompatibility of silica coated NaYF₄ upconversion fluorescent nanocrystals. *Biomaterials*. 2008; 29 (30): 4122-8.
- 37 Johnson NJJ, Sangeetha NM, Boyer J-C, Veggel FCJM van. Facile ligand-exchange with polyvinylpyrrolidone and subsequent silica coating of hydrophobic upconverting β-NaYF₄:Yb³⁺/Er³⁺ nanoparticles. *Nanoscale*. 2010; 2 (5): 771-7.
- 38 Li Z, Zhang Y, Shuter B, Muhammad Idris N. Hybrid lanthanide nanoparticles with paramagnetic shell coated on upconversion fluorescent nanocrystals. *Langmuir*. 2009; 25 (20): 12015-8.
- 39 Jana NR, Earhart C, Ying JY. Synthesis of water-soluble and functionalized nanoparticles by silica coating. *Chemistry of Materials*. 2007; 19 (21): 5074-82.
- 40 Park JC, Gilbert DA, Liu K, Louie AY. Microwave enhanced silica encapsulation of magnetic nanoparticles. *Journal of Materials Chemistry*. 2012; 22 (17): 8449-54.
- 41 Salgueiriño-Maceira V, Correa-Duarte MA, Spasova M, Liz-Marzán LM, Farle M. Composite silica spheres with magnetic and luminescent functionalities. *Advanced Functional Materials*. 2006; 16 (4): 509-14.
- 42 Mader HS, Link M, Achatz DE, Uhlmann K, Li X, Wolfbeis OS. Surface-modified upconverting microparticles and nanoparticles for use in click chemistries. *Chemistry - A European Journal*. 2010; 16 (18): 5416-24.
- 43 Ehlert O, Thomann R, Darbandi M, Nann T. A four-color colloidal multiplexing nanoparticle system. *ACS Nano*. 2008; 2 (1): 120-4.
- 44 Sivakumar S, Diamante PR, van Veggel FCJM. Silica-coated Ln³⁺-Doped LaF₃ Nanoparticles as robust down- and upconverting biolabels. *Chemistry - A European Journal*. 2006; 12 (22): 5878-84.
- 45 Wang F, Liu X. Recent advances in the chemistry of lanthanide-doped upconversion nanocrystals. *Chemical Society Reviews*. 2009; 38 (4): 976-89.
- 46 Li Z, Zhang Y, Jiang S. Multicolor core/shell-structured upconversion fluorescent nanoparticles. *Advanced Materials*. 2008; 20 (24): 4765-9.
- 47 Mirsky VM, Riepl M, Wolfbeis OS. Capacitive monitoring of protein immobilization and antigen-antibody reactions on monomolecular alkythiol films on gold electrodes. *Biosensors and Bioelectronics*. 1997; 12 (9-10): 977-89.
- 48 Haase M, Schäfer H. Upconverting nanoparticles. *Angewandte Chemie International Edition*. 2011; 50 (26): 5808-29.
- 49 Qian H-S, Zhang Y. Synthesis of hexagonal-phase core-shell NaYF₄ nanocrystals with tunable upconversion fluorescence. *Langmuir*. 2008; 24 (21): 12123-5.
- 50 Sedlmeier A, Achatz DE, Fischer LH, Gorris HH, Wolfbeis OS. Photon upconverting nanoparticles for luminescent sensing of temperature. *Nanoscale*. 2012; 4 (22): 7090-6.
- 51 Miller SA, Rast HE, Caspers HH. Lattice vibrations of LiYF₄. *The Journal of Chemical Physics*. 1970; 52 (8): 4172-5.
- 52 Chen G, Ohulchanskyy TY, Kachynski A, Ågren H, Prasad PN. Intense visible and near-infrared upconversion photoluminescence in colloidal LiYF₄:Er³⁺ nanocrystals under excitation at 1490 nm. *ACS Nano*. 2011; 5 (6): 4981-6.
- 53 Suyver JF, Grimm J, van Veen MK, Biner D, Krämer KW, Güdel HU. Upconversion spectroscopy and properties of NaYF₄ doped with Er³⁺, Tm³⁺ and/or Yb³⁺. *Journal of Luminescence*. 2006; 117 (1): 1-12.
- 54 Liu GK, Chen XY, Zhuang HZ, Li S, Niedbala RS. Confinement of electron-phonon interaction on luminescence dynamics in nanophosphors of Er³⁺:Y₂O₃. *Journal of Solid State Chemistry*. 2003; 171 (1-2): 123-32.
- 55 Tandon P, Förster G, Neubert R, Wartewig S. Phase transitions in oleic acid as studied by X-ray diffraction and FT-Raman spectroscopy. *Journal of Molecular Structure*. 2000; 524 (1-3): 201-15.
- 56 Mayo DW, Foil FA, Hannah RW. Course notes on the interpretation of infrared and Raman spectra. Chichester, USA: John Wiley and Sons; 2004.
- 57 Breitsprecher D, Jaiswal R, Bombardier JP, Gould CJ, Gelles J, Goode BL. Rocket launcher mechanism of collaborative actin assembly defined by single-molecule imaging. *Science*. 2012; 336 (6085): 1164-8.
- 58 Sperling RA, Parak WJ. Surface modification, functionalization and bioconjugation of colloidal inorganic nanoparticles. *Philosophical Transactions of the Royal Society A*. 2010; 368 (1915): 1333-83.
- 59 Schasfoort RBM, Tudos AJ, Schasfoort RBM, Tudos AJ. *Handbook of Surface Plasmon Resonance*. Cambridge, UK: Royal Society of Chemistry; 2008.
- 60 Liebherr RB, Soukka T, Wolfbeis OS, Gorris HH. Maleimide activation of photon upconverting nanoparticles for bioconjugation. *Nanotechnology*. 2012; 23 (48): 485103.